Long-term follow-up of lung biodistribution and effect of instilled SWCNTs using multiscale imaging techniques

Article *in* Nanotechnology · April 2010

DOI: 10.1088/0957-4484/21/17/175103 · Source: PubMed

CITATIONS
15

READS
87

6 authors, including:

Achraf Al Faraj
American University of Science and Technology
43 PUBLICATIONS **519** CITATIONS

SEE PROFILE

Amine Bessaad
Saad Dahlab University
14 PUBLICATIONS **173** CITATIONS

SEE PROFILE

Emmanuelle Canet-Soulas
Claude Bernard University Lyon 1
145 PUBLICATIONS **2,047** CITATIONS

SEE PROFILE

Yannick Crémillieux
University of Bordeaux
93 PUBLICATIONS **1,600** CITATIONS

SEE PROFILE

Long-term follow-up of lung biodistribution and effect of instilled SWCNTs using multiscale imaging techniques

2010 Nanotechnology 21 175103

(http://iopscience.iop.org/0957-4484/21/17/175103)

Nanotechnology **21** (2010) 175103 (9pp) doi:10.1088/0957-4484/21/17/175103

Long-term follow-up of lung biodistribution and effect of instilled SWCNTs using multiscale imaging techniques

Achraf Al Faraj[1], Amine Bessaad[1], Katarzyna Cieslar[1], Ghislaine Lacroix[2], Emmanuelle Canet-Soulas[1] and Yannick Crémillieux[1,3]

[1] Université Lyon1, CREATIS-LRMN, CNRS 5220, INSERM U630, Lyon, France
[2] Institut National de l'Environnement et des Risques Industriels (INERIS), Verneuil-en-Halatte, France

E-mail: yannick.cremillieux@univ-lyon1.fr

Received 26 October 2009, in final form 3 March 2010
Published 6 April 2010
Online at stacks.iop.org/Nano/21/175103

Abstract

Due to their distinctive properties, single-walled carbon nanotubes (SWCNTs) are being more and more extensively used in nanotechnology, with prospects in nanomedicine. It would therefore appear essential to develop and apply appropriate imaging tools for detecting and evaluating their biological impacts with the prospect of medical applications or in the situation of accidental occupational exposure. It has been shown recently that raw SWCNTs with metallic impurities can be noninvasively detected in the lungs by hyperpolarized ^{3}helium (HP-^{3}He) MRI. Moreover raw and purified SWCNTs had no acute biological effect. The purpose of the present longitudinal study was to investigate long-term follow-up by imaging, as well as chronic lung effects.

In a 3-month follow-up study, multiscale imaging techniques combining noninvasive HP-^{3}He and proton (H) MRI to *ex vivo* light (histopathological analysis) and transmission electron microscopy (TEM) were used to assess the biodistribution and biological effects of intrapulmonary instilled raw SWCNTs. Specific *in vivo* detection of carbon nanotubes with MRI relied on their intrinsic metal impurities. MRI also has the ability to evaluate tissue inflammation by the follow-up of local changes in signal intensity. MRI and *ex vivo* microscopy techniques showed that granulomatous and inflammatory reactions were produced in a time and dose dependent manner by instilled raw SWCNTs.

1. Introduction

Single-walled carbon nanotubes (SWCNTs) with their unique nanometer-scale structure and their fascinating mechanical, electric and thermal properties are being more and more extensively used for different applications in nanotechnology, including in nanomedicine [1]. Their high aspect ratio (ratio of length to width) makes them an attractive structural material, but their nanometer-scale diameter and needle-like shape highlight the importance of identifying rapidly the potential hazards of these materials [2, 3]. Knowledge of the potential pathogenic mechanisms of CNTs is necessary to minimize the danger to exposed individuals [4].

Data on the biological impacts of CNTs *in vivo* are poor and contradictory; however, the majority of research performed on cellular or post-mortem models has demonstrated that CNTs can produce potential health problem after pulmonary exposure [5–8]. Appropriate methods are needed to study their biodistribution and biological impacts *in vivo* after administration to living species, in particular noninvasive imaging techniques.

[3] Address for correspondence: Université Lyon 1, CREATIS-LRMN, UMR CNRS 5220, U630 INSERM, ESCPE, Campus La Doua, Bâtiment 308, 43 Boulevard du 11 Novembre, 69622 Villeurbanne Cedex, France.

Magnetic resonance imaging (proton MRI) has several advantages over competing noninvasive modalities with respect to spatial and temporal resolution, the range and specificity of functional measures available, and the lack of repeated exposure to ionizing radiation during longitudinal studies. However, because of magnetic susceptibility due to the heterogeneity of microscopic structures (air–tissue interfaces) and because of their weak proton density, the lung remains a difficult organ to image with proton MRI. With the introduction of hyperpolarized (HP) gases (i.e. ^{3}He, ^{129}Xe) acting as contrast agents that diffuse rapidly to fill the airspaces of the lungs and allow visualization and measurement of the ventilated airways and alveolar spaces, pulmonary ventilation imaging is possible [9–11].

Specific detection of CNTs in a biological environment can be performed *in vivo* using radio or fluorescent labels [12, 13], but these labels may gradually dissociate from the CNT or decay and lose activity over a short period of time. Direct detection of CNTs can be also performed *ex vivo* using their Raman spectroscopic signatures relying on their intrinsic physical properties rather than radiolabels or spectroscopic tags for indirect detection [14].

Similarly, one can certainly take advantage of different intrinsic metal impurities located at the surface or inside raw CNTs depending on the manufacture and synthesis methods (i.e. iron carbonyl serves as catalyst during the production process) or label CNTs with iron nanoparticles to allow their noninvasive *in vivo* detection using MRI.

Due to their strong magnetic moment, iron particles induce magnetic field inhomogeneities in their vicinity and attenuate the NMR signal of water molecules in surrounding tissues. With these contrast properties, CNT can be compared to standard MRI contrast agents used for cellular and molecular imaging in whole body MRI.

The application of injected and instilled iron nanoparticles as contrast agents acting on the ^{3}He NMR signal in the broncho-alveolar space has been previously demonstrated [15–17]. The presence of iron particles translates into local changes in the MR signal intensity of the ^{3}He ventilation image.

The purpose of this long-term study was to assess longitudinally the lung biodistribution and biological effect of intratracheally instilled SWCNTs in a rat model using multimodality–multiscale imaging techniques combining noninvasive hyperpolarized ^{3}helium (HP ^{3}He) magnetic resonance imaging (MRI) with noninvasive *in vivo* proton (H) MRI, *ex vivo* light (histopathological analysis) and transmission electron microscopy (TEM).

We have recently reported that SWCNTs with associated metal impurities can be detected noninvasively using HP ^{3}He MRI in a rat model [18]. The susceptibility effects induced by the metal impurities contained in the intrapulmonary instilled SWCNT samples were large enough to induce a significant drop in magnetic field homogeneity as detected in the ^{3}He MR images.

The absence of signal from healthy lung parenchyma in proton MR images in combination with a background free of artifacts provides a high contrast-to-noise ratio for the detection of fluid secretion related to inflammation and edema [19, 20] or to collagen deposition and atelectasis (hallmarks of fibrosis) [21].

Histopathological analysis, routinely used for *in vitro* and *in vivo* assessment of the toxicity of ultrafine particles, can be very useful in assessing the integrity of lung tissue and localizing CNT aggregates and any pathological effects (i.e. granuloma formation).

Finally, one of the great challenges in studying the impact of nanoparticles in the lung is their visualization within tissues or single cells at a sub-cellular scale. With its nanometric resolution, TEM provides an ideal tool to analyze CNT-related structural changes of the respiratory tract, to localize CNTs and to detect the presence of inflammatory cells produced in their presence and to investigate the nature of CNT–lung interactions [22].

2. Materials and methods

2.1. Physicochemical characteristics of SWCNTs

Prior to exposure, the SWCNTs were characterized by TEM using a 120 kV microscope (JEM 1400, JOEL) and their metal impurities were analyzed using inductively coupled plasma-mass spectrometry (ICP-MS). Samples were mineralized with 5 ml nitric acid and 5 ml hydrochloric acid in a microwave oven. Concentrations of 67 different metals were semi-quantitatively measured by ICP-MS (Elan 6100DRC, Perkin-Elmer, ON, Canada).

2.2. Study design

Six- to eight-week-old male Sprague-Dawley rats were obtained from Charles River (L'Arbresle, France). Animals were housed in the Lyon-1 University animal-care unit, a facility accredited by the local veterinary authority. They had free access to a conventional laboratory diet and water and were handled in accordance with official French guidelines for the care and use of laboratory animals.

Animals were anesthetized by intramuscular administration of 0.12 ml/100 g of the following mixture: 3.5 ml of ketamine (1000 mg ml^{-1}), 3 ml of xylazine (2%) and 1 ml of atropine (1 mg ml^{-1}). Atropine was used to reduce mucus secretion.

The numbers of animals in each group with the time of sacrifice for post-mortem analysis are provided in table 1.

Intratracheal instillation of CNTs was performed via an intratracheal plastic catheter after hyperventilation (ventilator model 683, Harvard Apparatus, Holliston, MA) for 30 s at 150 strokes min^{-1} (tidal volume = 2.5 ml).

2.3. HP ^{3}He lung MRI

2.3.1. Acquisition. HP-^{3}He lung ventilation imaging was performed on a 12 cm bore 2 T Oxford magnet (Oxford Magnet, Oxford, UK) with actively shielded gradients (180 mT m^{-1}) interfaced to an MRRS console (MRRS, Guildford, UK). An 8 cm diameter Alderman–Grant RF coil tuned to the ^{3}He frequency was used. ^{3}He polarization was

Table 1. Number of animals used in the different groups (with the instilled dose corresponding to each group) at the different investigation time point.

Groups	Short-term D1	Mid-term D7	Long-term D30	Very long-term D90	Total
Control (BSA–saline vehicle)	1	1	1	2	5
Low dose 0.1 mg (0.4 mg kg^{-1})	3	3	3	—	9
Mid-dose 0.5 mg (2 mg kg^{-1})	3	3	3	4	13
High dose 1 mg (4 mg kg^{-1})	3	3	3	—	9

achieved by spin-exchange optical pumping. End polarization levels between 20% and 30% were obtained [23]. Ventilation images were acquired using a free-breathing imaging protocol to avoid repeated intubation. A breathing mask was fitted on the rat's head and the animal was allowed to breathe freely from the ^{3}He reservoir during the 20 s image acquisition [24].

Pulmonary ventilation images using a radial sequence were acquired with an echo time (TE) of 1 ms which shows a good compromise between image quality and sensibility to simultaneously evaluate ventilation and lung susceptibility effects after iron-containing CNT deposition [17]. A total of 200 radial projections with 128 samples were acquired per image. The repetition time was 10 ms, the field of view (FOV) was 80 mm and a flip angle was 30°. The pulmonary imaging protocol was performed 24 h, 7 days and 30 days after exposure.

2.3.2. Image reconstruction and analysis. Image reconstruction and analysis were carried out using IDL software (RSI, Boulder, CO). Ventilation images were reconstructed using a retrospective cine approach [24] with synchronization of the image acquisition with the breathing pattern of the animal. Each reconstructed ventilation image corresponded to a 100 ms time window.

For the measurement of the image signal-to-noise ratio (SNR) and coefficient of variation (CV) to assess the homogeneity of lung images, the maximal intensity grayscale image, corresponding to the end-inspiration breathing cycle, was selected to visualize the largest fraction of ventilation airspaces. A region of interest (ROI) encompassing the right and left lung was manually selected.

2.4. Proton lung MRI

2.4.1. Acquisition. Proton lung imaging was performed on a 10 cm bore actively shielded 4.7 T Bruker magnet (Bruker Biospin GmbH, Rheinstetten, Germany) interfaced to ParaVision software for preclinical MR imaging research. A Bruker transmission and reception proton volume RF coil was used, providing good RF homogeneity over the volume of interest.

A gradient echo sequence (TR/TE = 7/3.6 ms) with the following parameters was used: field-of-view (FOV) 6 cm × 6 cm, flip angle 15°, matrix size 256 × 128, bandwidth 70 kHz and slice thickness of 1.5 mm. A single-slice image was obtained by computing the 2D Fourier transform (FT) of the averaged signal from 45 individual image acquisitions and interpolating the data set to 256 pixels × 256 pixels. A tube containing gadolinium solution used as a reference was positioned on the rat's chest to enable contrast-to-noise ratio (CNR) measurement and proton MR signal normalization.

2.4.2. Image analysis. To monitor inflammation events in the lung, the number of hyper-intensity pixels (blood vessel and edema) was assessed in lung parenchyma using IDL software on the set of proton MRI images corresponding to each rat. Since the signals from injured lung regions and vessels were of comparable intensities, hyper-intensity pixels corresponding to the vessels were subtracted from the volumes determined on post-challenge images [19] and an average percentage increase in the set of axial images was calculated for each rat. The segmentation parameters were the same for all the analyzed images, chosen to segment regions corresponding to high intensity signals. Threshold was chosen to include all apparent fluid signal in lung parenchyma.

2.5. Lung histopathology

At different investigation time points (table 1), lungs were removed and fixed by filling with 4% para-formaldehyde (PFA) to an airway pressure of 25 cm H_2O. They were then dehydrated and embedded in paraffin. Five-micrometer transverse sections were cut (Leica 2045 microtome) and stained with hematoxylin–eosin–saffron (HES) for general morphology and the assessment of the dispersion of nanotubes.

HES is a routine staining which provides excellent contrast between elastic fibers, cytoplasm and connective tissues and allows assessment of the integrity of the lung tissue and additionally localizes CNT aggregates which are detectable without any specific coloration. The hematoxylin stains cell nuclei (dark blue), the eosin stains the cytoplasm (red), and the saffron stains collagen and connective tissue (yellow).

2.6. Transmission electron microscopy

Small portion of lung corresponding to each group were removed and chemically fixed for conventional TEM. Briefly, the specimen was immediately covered with 4% glutaraldehyde (GA) in 0.2 M cacodylate buffer pH 7.4, cut in 1 mm^3 pieces and fixed for 2 h at 4 °C in the same fixative medium. Samples were then rinsed three times in 0.4 M saccharose and 0.2 M cacodylate buffer and postfixed for 2 h in 2% osmium tetroxide in the same buffer after one night in vacuum bell jar. This procedure was followed by dehydration in graded ethanol and embedding in Epon. Ultrathin sections

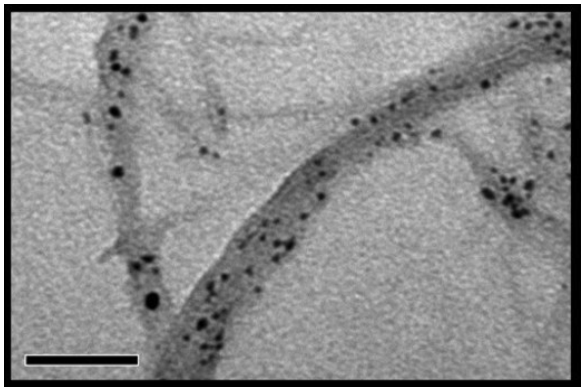

Figure 1. Transmission electron micrograph of SWCNT showing the presence of impurities (black dots) and the structural shape of SWCNT bundles. The scale bar represents 50 nm.

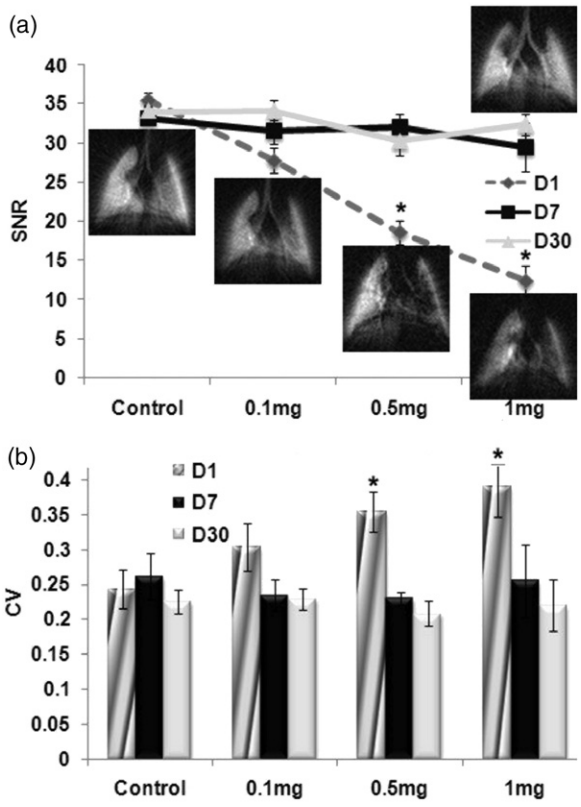

Figure 2. (a) Signal-to-noise ratio (SNR) variation of ^{3}He lung ventilation images for the different groups at D1, D7 and D30 with the corresponding images for all the groups (control, 0.1 mg, 0.5 mg and 1 mg) at D1 and an example of the 1 mg instilled group at D30. (b) Coefficient of variation (CV) for all the groups for different MRI protocol investigation times. *Statistically different from control group ($p < 0.05$).

were contrasted with methanolic uranyl acetate (30 min) and lead citrate (10 min) and observed under a 120 kV transmission electron microscope (JEOL JEM 1400) equipped with Gatan Orius CCD camera.

2.7. Statistical analyses

All data are expressed as means ± SD. Non-parametric statistical tests (SPSS, SPSS Inc, Chicago, IL) were performed;

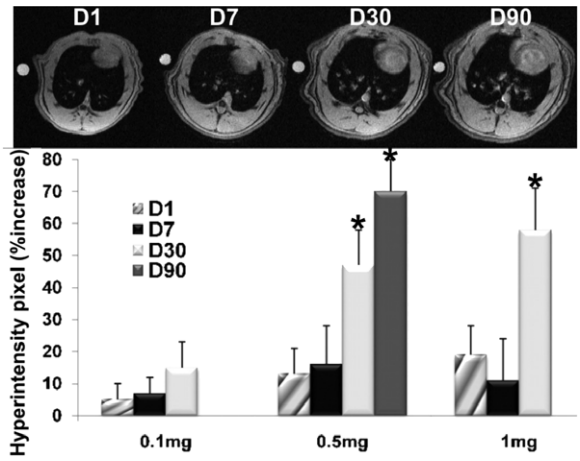

Figure 3. Top: MR images for the 0.5 mg instilled group at different investigation times at approximately the same slice position. Bottom: histogram of hyper-intensity pixels (% increase per image) compared to control proton lung images showing an increase of hyper-signal pixels due to the presence of inflammatory regions at D30 and D90. *Statistically different from control group ($p < 0.05$).

the Kruskal–Wallis test for unpaired groups and the Friedman test for comparison between time. A p value <0.05 was considered significant for all tests.

3. Results and discussion

The supplied SWCNTs (CNI® Buckytubes, Houston, TX, USA) used in this study were produced by chemical vapor deposition (CVD) by means of the high-pressure carbon monoxide (HiPCO) process, a commonly used technology in the manufacture of SWCNTs synthesized using a metal catalyst. Thus raw SWCNTs usually contain significant amounts (10% by weight in our case) of iron that may have the potential to cause additional toxic effects, but could also be detected *in vivo* using MRI (figure 1).

The lung is the prime target for deposition of SWCNTs, as they can be inhaled during technological processing and use. Intratracheal instillation (ITI) was preferred in our feasibility study because it is a reproducible administration technique in the lung allowing accurate control of the suspension dose administered. Indeed, ITI is the most suitable technique for pulmonary absorption and deposition studies where dosage precision is of prime concern [25]. When administered by ITI, the bolus of particle suspension enters deeper into the rats' lungs during breathing after hyperventilation.

In the current 3-month longitudinal study (measurements performed at day 1 (D1), day 7 (D7), day 30 (D30) and day 90 (D90)), rats were divided in different groups (table 1) and received a single bolus (0, 0.1, 0.5 or 1 mg) of SWCNT suspension. Upon administration to the animals, CNT powder was suspended in 150 μl saline solution (NaCl 0.9%) containing bovine serum albumin (BSA) to obtain a homogeneous and better dispersed CNT solution after at least 10 min sonication in an ultrasonic bath [26].

Body weight was assessed throughout the experimental schedule to monitor the general health of the animals exposed

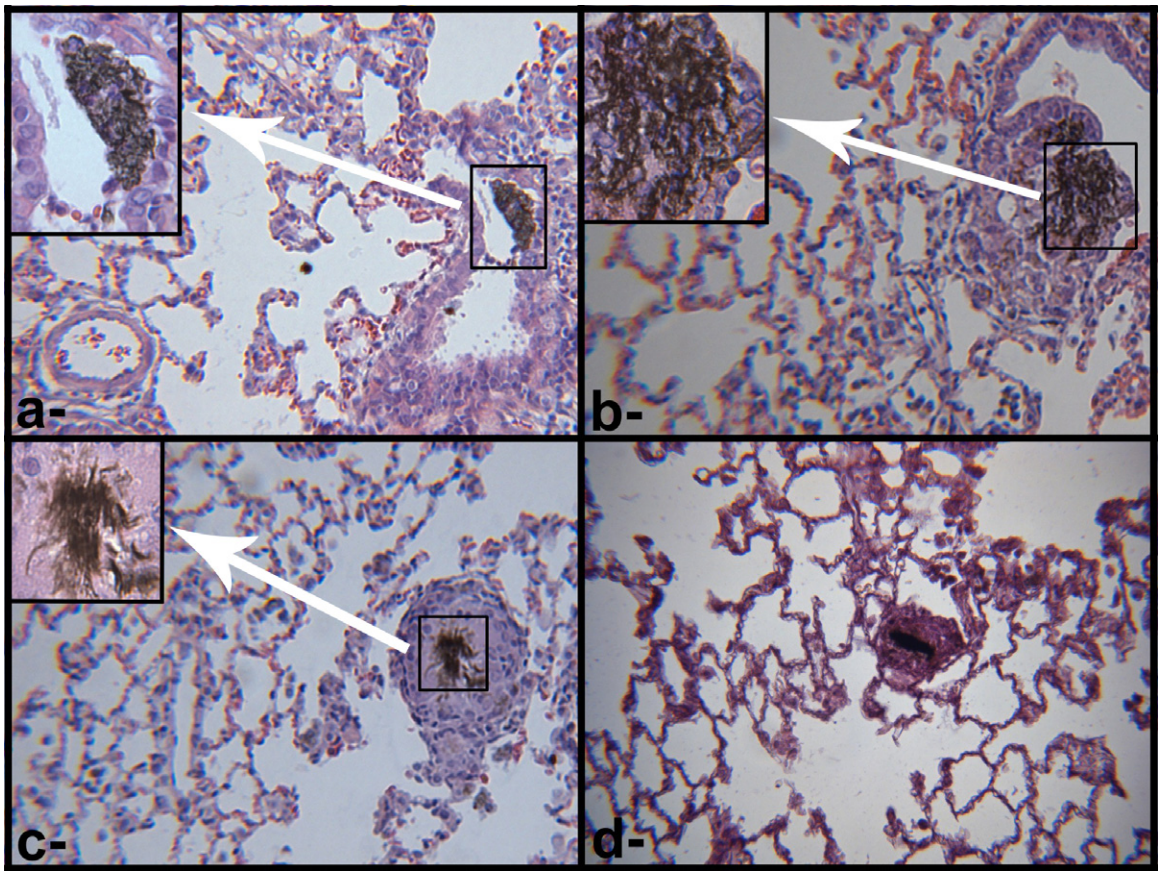

Figure 4. Representative HES histopathological lung images after 0.5 mg (2 mg kg^{-1}) intratracheal instillation of SWCNTs in a rat model. Dose and time dependent inflammatory responses characterized by interstitial granulomas located beneath the bronchial epithelium were induced after SWCNT persistence. (a) At an early time point (D1), SWCNTs were found in the lumen of bronchioles and alveoli without evidence of epithelial damage. (b) At a mid-time point (D7), SWCNT aggregates tend to infiltrate neighboring lung interstitium inducing a mononuclear cell infiltrate. (c) At a long time point (D30), multifocal granulomatous reactions (giant cells) were present around the sites of SWCNT deposition. (d) At a very long time point (D90), granulomatous reaction persisted with SWCNT deposition, with membrane thickening and alveolar collapses occurring. Original magnification: 100× (400× in zoomed regions).

(This figure is in colour only in the electronic version)

to SWCNTs. Upon instillation, and throughout the entire study, no unusual behaviors or differences between groups were observed. Starting with a weight of 250 ± 10 g (n = 36), the treated animals had a normal weight gain, weighing 540 ± 6 g (n = 6) at the completion of the 3-month follow-up study, identical to controls.

HP-^{3}He MR imaging performed under a free-breathing protocol [24] exhibited dose dependent hypo-intense and void signal regions in the short-term (D1) imaging period with a signal-to-noise (SNR) decrease and coefficient of variation (CV) increase ($p < 0.05$) observed in lung images (figure 2).

At mid- and long-term investigations points (D7 and D30), HP ^{3}He lung images show homogeneous ventilation patterns with a SNR and CV statistically comparable to control images. The observed signal recovery with time might be related to encapsulation of SWCNT bundles, homogenization of SWCNT distribution and incorporation of iron impurities in ferritin molecules or in hemosiderin deposits.

No ventilation defects were observed in the lung of any animals throughout the longitudinal study and no SWCNTs were detected in systemic organs susceptible to accumulate or eliminate particles (liver, spleen and kidneys) using systemic proton MRI and histopathology as shown in a previous study [18].

Proton lung MR imaging was also performed using a free-breathing protocol by an image averaging technique providing sufficiently suppressed cardiac and respiratory motion artifacts and having the advantage of being less time-consuming and more adapted for routine applications than cardio-respiratory triggered MR imaging [27].

One month after SWCNT exposition, proton MRI revealed the presence of some hyper-intensity pixels ($p < 0.05$) which can be related to small detectable inflammatory nodules in animal groups instilled with 0.5 and 1 mg of SWCNTs and to the same degree in the 0.5 mg SWCNT instilled group after 3 months (figure 3).

No acute inflammatory effects induced by the presence of SWCNTs in the pleura were detected using MRI [28].

To provide an in-depth and complementary view on the biological impacts of CNTs, lungs were carefully examined for tissue changes associated with nanotube deposition and their

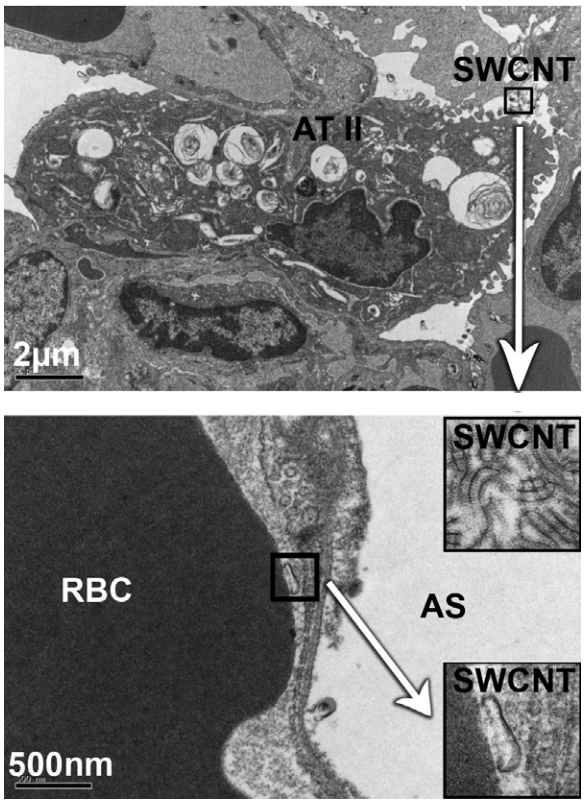

Figure 5. TEM micrograph at an early time point (D1) after 0.5 mg (2 mg kg^{-1}) instillation of SWCNTs showing: top, SWCNT in interaction with surfactant proteins or alveolar proteinase (zoomed image) exposed to alveolar epithelial type II (ATII); bottom, SWCNTs traversing the wall of capillary vessel and in direct contact with a red blood cell. AT II, alveolar epithelial type II; RBC, red blood cell; AS, alveolar space.

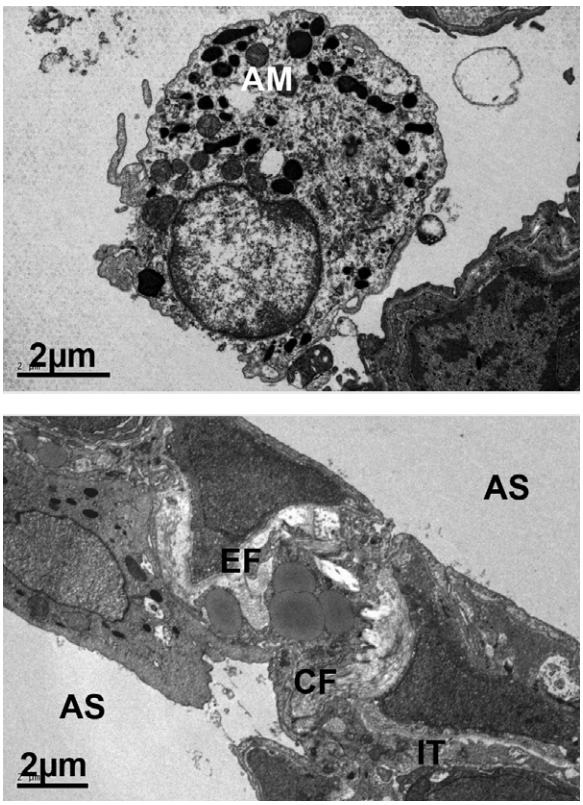

Figure 6. TEM micrograph at the mid-time point (D7) after 0.5 mg (2 mg kg^{-1}) instillation of SWCNTs showing an activation of: top, alveolar macrophages (AM) in the presence of SWCNTs; bottom, interstitial cells around the site of SWCNT deposition. AM, alveolar macrophage; AS, alveolar space; EF, elastic fibers; CF, collagen fibers; IT, interstitium.

nanotoxicity at a microscopic scale using light microscopy on HES stained histopathological lung slices (figure 4).

At an early stage (D1), SWCNT aggregates were found in the lumen of bronchioles and alveoli without evidence of epithelial damage or inflammation for all exposed doses (0.1, 0.5 and 1 mg). An increased number of SWCNTs was qualitatively correlated on light microscopic images with exposure concentrations.

Although the sonication and addition of albumin were taken into consideration before instillation to obtain a homogeneous distribution due to the poor solubility and van der Waals interaction of the SWCNTs, they tend to aggregate into clumps in bronchioles and alveoli.

At the mid-stage time point (D7), the alveolar septa became thicker and SWCNT aggregates formed a pellicle firmly adhering to the bronchiolar wall which tended to penetrate the wall and infiltrate neighboring lung interstitium, inducing a mononuclear cell infiltrate (figure 4).

The effects persisted and progressed to give rise to a multifocal granulomatous reaction containing macrophages, lymphocytes, fibroblasts and collagen deposition around the sites of SWCNT deposition at the late stage investigation time point (D30) and to the same degree at the very late stage (D90), with membrane thickening and alveolar collapses present due to bio-persistence of SWCNTs.

With the increase in the SWCNT dose, collagen deposition and pulmonary fibrosis, which are typical features following inflammatory response, became more severe. Pneumonitis, characterized by a peribronchiolar accumulation of polymorphonuclear neutrophils (PMN) and the appearance of granulomatous lesions, was observed in the different histopathological lung slices.

Even with the lowest exposure dose (0.1 mg) corresponding to 0.4 mg kg^{-1}, production of an inflammatory response around the site of SWCNT deposition was observed in histological slices.

The dose dependent inflammatory responses observed at each time point after SWCNT instillation in rats, being the evidence of a foreign tissue body reaction, is in accordance with different CNT-related studies [5, 29–31].

No inflammatory process in the pleura was observed by means of the histopathological analysis, in agreement with the proton lung MR readouts.

Encapsulation of SWCNT bundles with the formation of multifocal granulomas observed 1 week after exposure might have had the result of preventing direct contact of the SWCNT iron impurities with HP gases in lung alveoli, confirming the transient effect on SNR observed in HP ^{3}He MRI. The accentuation of inflammatory effects with collagen fiber deposition and giant cell formation 1 month after exposure can explain the hyper-intense pixels observed in proton lung MRI.

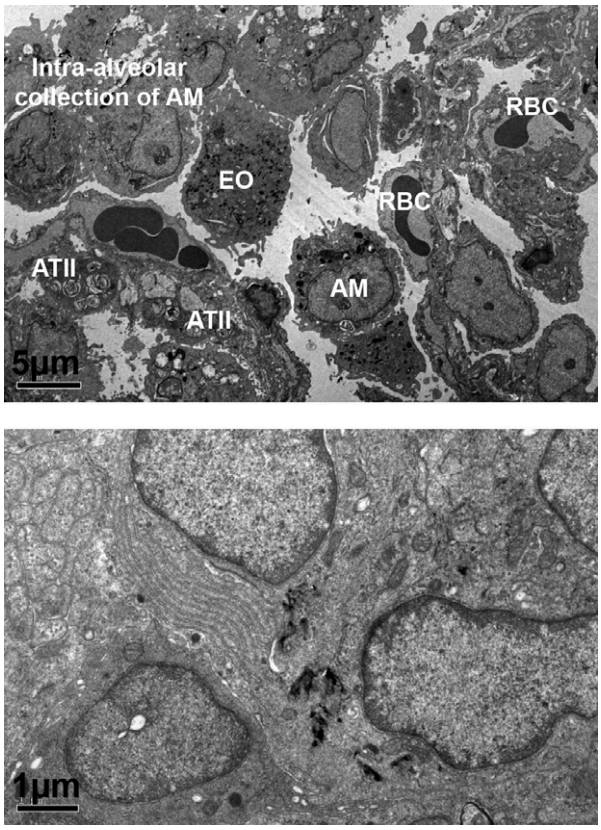

Figure 7. TEM micrograph at late time point (D30) after 0.5 mg (2 mg kg^{-1}) instillation of SWCNTs showing an amplification of the inflammatory reaction and severe granulomatous lesions characterized by the presence of: top, an increased number of inflammatory cells (ATII, AM, EO); bottom, collagen deposition with persistence of SWCNTs. AT II, alveolar epithelial type II; AM, alveolar macrophages; EO, eosinophil; RBC, red blood cell.

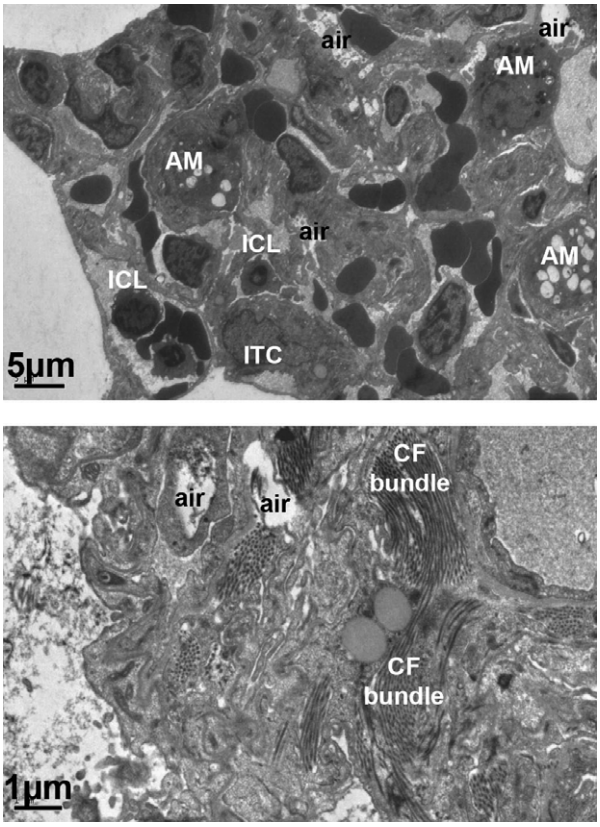

Figure 8. TEM micrograph at the very late time point (D90) after 0.5 mg (2 mg kg^{-1}) instillation of SWCNTs showing alveolar collapses and wall thickening with abundant alveolar macrophage activation and an emphysema-like phenotype. AM, alveolar macrophages; ICL, intra-capillary lymphocyte; ITC, interstitial cell; CF, collagen fiber.

Even histopathological analysis is limited in localizing non-aggregated SWCNTs and assessing their biological effect at a sub-cellular level. SWCNT aggregates producing inflammatory granulomas may have different effects when they are more homogeneously distributed in the lungs after inhalation. The ultra-structural features of the lung tissue were observed by TEM which provides an ideal tool for analyzing SWCNT-related sub-structural changes in the lung and for understanding the inflammatory process after SWCNT deposition.

At an early time point, SWCNTs reaching the gas-exchange region of the alveoli were found to interact with surfactant proteins and alveolar proteinase or to be exposed to different cells including alveolar epithelial type II (AT II) or alveolar macrophages (AM) [8]. A significant increase of alveolar type II cells, the progenitor cells that replicate following the death of alveolar type I cells, was detected (figure 5).

Some of the SWCNTs instilled in the alveolar spaces could also have the potential to traverse the wall of the capillary vessels downstream and to 'invade' other organs and be detected in liver, spleen and kidneys. However, such an effect was not observed, as reported for the intrapulmonary instillation of 0.5 mg of SWCNTs in a previous study [18]. Therefore, it can be assumed that the passage of intrapulmonary instilled SWCNTs into the blood circulation is limited or their uptake by systemic organs is absent.

One week after instillation, a significant increase in activated alveolar macrophages which form the first line of defense against foreign materials in many tissues and an activation of interstitial cells were detected in lung tissue around the site of SWCNT deposition (figure 6).

At the 1-month time point, an amplification of the inflammatory reaction and a severe granulomatous lesion were assessed by TEM (figure 7), in accordance with the giant cells detected by light microscopy. At the very late investigation time point, alveolar collapses and wall thickening with abundant alveolar macrophage activation were observed (figure 8).

4. Conclusion

Noninvasive HP-^{3}He and proton MRI combined with *ex vivo* optical microscopy and TEM represent powerful multimodality imaging techniques allowing in-depth characterization of the biodistribution and long-term biological impacts of iron-containing SWCNTs.

After intrapulmonary instillation in a rat model, raw SWCNTs were found to produce granulomatous and inflammatory reactions in a time and dose dependent manner. These findings, in addition to their bio-persistence, suggest an increased risk of developing lung cancer and the overall toxicity of the nanoparticles used in the present study, i.e. with metallic impurities.

Similar studies have to be performed on different types of CNT or ultrafine related particles on different animal models and under different exposure conditions (i.e. inhalation) to obtain a comparable full characterization of their nanotoxicity and identify physicochemical properties that influence their deposition and potential health effects (i.e. impurities, fiber length, chemical stability, . . .).

Acknowledgments

This work was supported by the French ANR through RESPINTTOX project (SEST program), the French Ministry of Education and Research, and the European Union Marie Curie Research Training Network PHeLINet contract number MRTN-CT-2006-036002.

References

[1] Baughman R H, Zakhidov A A and de Heer W A 2002 Carbon nanotubes—the route toward applications *Science* **297** 787–92

[2] Helland A, Wick P, Koehler A, Schmid K and Som C 2007 Reviewing the environmental and human health knowledge base of carbon nanotubes *Environ. Health Perspect.* **115** 1125–31

[3] Service R F 2004 Nanotoxicology. Nanotechnology grows up *Science* **304** 1732–4

[4] Maynard A D *et al* 2006 Safe handling of nanotechnology *Nature* **444** 267–9

[5] Lam C W, James J T, McCluskey R and Hunter R L 2004 Pulmonary toxicity of single-wall carbon nanotubes in mice 7 and 90 days after intratracheal instillation *Toxicol. Sci.* **77** 126–34

[6] Chou C C, Hsiao H Y, Hong Q S, Chen C H, Peng Y W, Chen H W and Yang P C 2008 Single-walled carbon nanotubes can induce pulmonary injury in mouse model *Nano Lett.* **8** 437–45

[7] Donaldson K, Aitken R, Tran L, Stone V, Duffin R, Forrest G and Alexander A 2006 Carbon nanotubes: a review of their properties in relation to pulmonary toxicology and workplace safety *Toxicol. Sci.* **92** 5–22

[8] Shvedova A A *et al* 2005 Unusual inflammatory and fibrogenic pulmonary responses to single-walled carbon nanotubes in mice *Am. J. Physiol.* **289** 698–708

[9] Driehuys B and Hedlund L W 2007 Imaging techniques for small animal models of pulmonary disease: MR microscopy *Toxicol. Pathol.* **35** 49–58

[10] Albert M S, Cates G D, Driehuys B, Happer W, Saam B, Springer C S Jr and Wishnia A 1994 Biological magnetic resonance imaging using laser-polarized 129Xe *Nature* **370** 199–201

[11] Driehuys B, Cofer G P, Pollaro J, Mackel J B, Hedlund L W and Johnson G A 2006 Imaging alveolar-capillary gas transfer using hyperpolarized 129Xe MRI *Proc. Natl Acad. Sci. USA* **103** 18278–83

[12] Lewin M, Carlesso N, Tung C H, Tang X W, Cory D, Scadden D T and Weissleder R 2000 Tat peptide-derivatized magnetic nanoparticles allow in vivo tracking and recovery of progenitor cells *Nat. Biotechnol.* **18** 410–4

[13] Liu Z, Cai W, He L, Nakayama N, Chen K, Sun X, Chen X and Dai H 2007 *In vivo* biodistribution and highly efficient tumour targeting of carbon nanotubes in mice *Nat. Nanotechnol.* **2** 47–52

[14] Liu Z, Davis C, Cai W, He L, Chen X and Dai H 2008 Circulation and long-term fate of functionalized, biocompatible single-walled carbon nanotubes in mice probed by Raman spectroscopy *Proc. Natl Acad. Sci. USA* **105** 1410–5

[15] Viallon M, Berthezene Y, Decorps M, Wiart M, Callot V, Bourgeois M, Humblot H, Briguet A and Cremillieux Y 2000 Laser-polarized $^{(3)}$He as a probe for dynamic regional measurements of lung perfusion and ventilation using magnetic resonance imaging *Magn. Reson. Med.* **44** 1–4

[16] Vignaud A, Maitre X, Guillot G, Durand E, de Rochefort L, Robert P, Vives V, Santus R and Darrasse L 2005 Magnetic susceptibility matching at the air–tissue interface in rat lung by using a superparamagnetic intravascular contrast agent: influence on transverse relaxation time of hyperpolarized helium-3 *Magn. Reson. Med.* **54** 28–33

[17] Al Faraj A, Lacroix G, Alsaid H, Elgrabi D, Stupar V, Robidel F, Gaillard S, Canet-Soulas E and Cremillieux Y 2008 Longitudinal 3He and proton imaging of magnetite biodistribution in a rat model of instilled nanoparticles *Magn. Reson. Med.* **59** 1298–303

[18] Al Faraj A, Cieslar K, Lacroix G, Gaillard S, Canet-Soulas E and Crémillieux Y 2009 *In vivo* imaging of carbon nanotubes biodistribution using MRI *Nano Lett.* **9** 1023–7

[19] Beckmann N, Tigani B, Ekatodramis D, Borer R, Mazzoni L and Fozard J R 2001 Pulmonary edema induced by allergen challenge in the rat: noninvasive assessment by magnetic resonance imaging *Magn. Reson. Med.* **45** 88–95

[20] Tigani B, Schaeublin E, Sugar R, Jackson A D, Fozard J R and Beckmann N 2002 Pulmonary inflammation monitored noninvasively by MRI in freely breathing rats *Biochem. Biophys. Res. Commun.* **292** 216–21

[21] Karmouty-Quintana H, Cannet C, Zurbruegg S, Ble F X, Fozard J R, Page C P and Beckmann N 2007 Bleomycin-induced lung injury assessed noninvasively and in spontaneously breathing rats by proton MRI *J. Magn. Reson. Imaging* **26** 941–9

[22] Muhlfeld C, Rothen-Rutishauser B, Vanhecke D, Blank F, Gehr P and Ochs M 2007 Visualization and quantitative analysis of nanoparticles in the respiratory tract by transmission electron microscopy *Part. Fibre Toxicol.* **4** 11

[23] Stupar V, Berthezene Y, Canet E, Tournier H, Dupuich D and Cremillieux Y 2003 Helium3 polarization using spin exchange technique: application to simultaneous pulmonary ventilation/perfusion imaging in small animals *Invest. Radiol.* **38** 334–40

[24] Stupar V, Canet-Soulas E, Gaillard S, Alsaid H, Beckmann N and Cremillieux Y 2007 Retrospective cine 3He ventilation imaging under spontaneous breathing conditions: a non-invasive protocol for small-animal lung function imaging *NMR Biomed.* **20** 104–12

[25] Leong B K, Coombs J K, Sabaitis C P, Rop D A and Aaron C S 1998 Quantitative morphometric analysis of pulmonary deposition of aerosol particles inhaled via intratracheal nebulization, intratracheal instillation or nose-only inhalation in rats *J. Appl. Toxicol.* **18** 149–60

[26] Elgrabli D, Abella-Gallart S, Aguerre-Chariol O, Robidel F, Rogerieux F, Boczkowski J and Lacroix G 2007 Effect of BSA on carbon nanotube dispersion for *in vivo* and *in vitro* studies *Nanotoxicology* **1** 266–78

[27] Beckmann N, Tigani B, Mazzoni L and Fozard J R 2001 MRI of lung parenchyma in rats and mice using a gradient-echo sequence *NMR Biomed.* **14** 297–306

[28] Quintana H K, Cannet C, Schaeublin E, Zurbruegg S, Sugar R, Mazzoni L, Page C P, Fozard J R and Beckmann N 2006 Identification with MRI of the pleura as a major site of the acute inflammatory effects induced by ovalbumin and endotoxin challenge in the airways of the rat *Am. J. Physiol.* **291** 651–7

[29] Liu A, Sun K, Yang J and Zhao D 2008 Toxicological effects of multi-wall carbon nanotubes in rats *J. Nanopart. Res.* **10** 1303–7

[30] Muller J, Huaux F and Lison D 2006 Respiratory toxicity of carbon nanotubes: How worried should we be? *Carbon* **44** 1048–56

[31] Carrero-Sanchez J C, Elias A L, Mancilla R, Arrellin G, Terrones H, Laclette J P and Terrones M 2006 Biocompatibility and toxicological studies of carbon nanotubes doped with nitrogen *Nano Lett.* **6** 1609–16